RSC Advances

PAPER

Published on 03 April 2025
Licensed under CC-BY-NC 4.0

Check for updates

Cite this: *RSC Adv.*, 2025, **15**, 10257

Luminescent down-shifting layers based on an isoquinoline-Eu(III) complex for enhanced efficiency of c-Si solar cells under extreme UV radiation conditions†

Darío Espinoza,[a] Ronald Nelson,[a] Fabian Vargas,[a] Alifhers Mestra,[a] Laura Sánchez-Muñoz,[b] Pere Alemany,[b] Douglas Olivares,[c] Luis Conde[d] and Jaime Llanos *[a]

The Atacama Desert's extreme UV radiation impacts photovoltaic devices, reducing silicon solar cell efficiency through overheating and photodegradation. To address this, we integrated a europium complex derived from 1-(diphenylphosphoryl)-3-isoquinolinecarboxylic acid into a polyvinyl butyral (PVB) matrix, forming a luminescent down-shifting layer (LDSL) that converts UV radiation into visible light. This LDSL improves light harvesting and mitigates UV-induced degradation. After LDSL application, photovoltaic analysis of a c-Si cell showed significant enhancements: short-circuit current density (J_{sc}) increased from 28.82 to 34.69 mA cm^{-2}, open-circuit voltage (V_{oc}) rose from 630.6 to 635.7 mV, and the fill factor (FF) remained stable. Incident photon-to-current efficiency (IPCE) curves indicated better performance, particularly in the UVA range, with overall cell efficiency improving from 14.10% to 16.62% at higher Eu complex concentrations. Electrochemical impedance spectroscopy (EIS) revealed that the Eu complex improved charge transfer, reducing recombination losses. This approach demonstrates significant potential for enhancing solar cell performance in high-irradiance environments like the Atacama Desert.

Received 24th January 2025
Accepted 23rd March 2025

DOI: 10.1039/d5ra00584a

rsc.li/rsc-advances

1. Introduction

The Atacama Desert, located along the Pacific Coast of South America, presents a combination of climatic conditions such as high altitudes, low humidity, and minimal cloud cover, which result in an increased intensity of direct solar radiation exhibiting exceptionally high levels of ultraviolet (UV) irradiation.[1,2] Since the performance of photovoltaic (PV) devices is highly dependent on the spectral composition of the incident light, it is essential to consider the specific solar conditions of this region to properly choose the type of PV technology to be used. Traditional PV devices are typically optimized for maximum efficiency under standard testing conditions (STC), based on a reference spectrum that assumes a global air mass of 1.5 (AMG 1.5G).[3,4] However, the spectral distribution in the Atacama Desert, with high UV levels, deviates significantly from STCs, potentially affecting the efficiency of PV cells designed for more temperate regions.

The high intensities of UV radiation do not only affect the efficiency of solar cells, but also accelerate the degradation of the usual PV materials.[5–7] For silicon-based cells prolonged exposure to UV radiation induces the formation of defect states in the silicon lattice, as well as causing the yellowing or delamination of encapsulation materials and the degradation of antireflection coatings, ultimately reducing the overall efficiency and operational lifespan of the solar cells.[5,8,9] To mitigate these detrimental effects, it is crucial to protect the sensitive components of the PV devices or to convert the incident high-energy radiation into less harmful, longer wavelengths that can be utilized by the solar cells.

One promising approach to address these challenges involves the incorporation of luminescent compounds containing lanthanide ions (Eu^3, Tb^{3+}, Dy^{3+}, Pr^{3+}, Sm^{3+}, Tm^{3+}), which can absorb short-wavelength UV radiation and re-emit it at longer wavelengths.[10,11] However, due to the nature of the f–f electronic transitions, lanthanide ions typically exhibit low absorption coefficients in the UV-visible-NIR region, making direct absorption inefficient.[12,13] This limitation can be

[a]*Departamento de Química, Facultad de Ciencias, Universidad Católica del Norte, Avda. Angamos 0610, Antofagasta 1270709, Chile. E-mail: jllanos@ucn.cl; Tel: +56 552355615*

[b]*Departament de Ciència de Materials i Química Física, Institut de Química Teòrica i Computacional (IQTCUB), Universitat de Barcelona, Diagonal 647, 08028 Barcelona, Spain*

[c]*Centro de Desarrollo Energético Antofagasta, Universidad de Antofagasta, Avda. Angamos 601, Antofagasta 1270300, Chile*

[d]*Solar Energy Research Center, Universidad de Chile, Tupper 2007, 8370451 Santiago, Chile*

† Electronic supplementary information (ESI) available: Supplementary figures mass and IR spectra. See DOI: https://doi.org/10.1039/d5ra00584a

© 2025 The Author(s). Published by the Royal Society of Chemistry

mitigated by using lanthanide complexes with appropriate organic ligands that act as antennas or sensitizers absorbing the UV light efficiently and then transfer the energy to the lanthanide ions which re-emit it, resulting in a significantly enhanced luminescence.[14–17]

In practical applications, devices such as luminescent solar concentrators (LSCs) and down-shifting layers (LDSLs) have been explored as potential solutions to improve the performance of PV technologies. LSCs are particularly promising due to their ability to concentrate and convert diffuse UV light over a large area into a smaller, more intense beam directed at a solar cell. This not only increases the effective light intensity reaching the PV cell, but also minimizes losses due to recombination. LDSLs, in addition, are thin films applied directly to the surface of the PV cell that convert harmful UV light into wavelengths that are more efficiently absorbed by the silicon-based active layers, thereby enhancing the photocurrent generation. These optical modifications have also shown considerable potential in reducing the degradation of the encapsulant and other organic components in the PV cell.[18–21]

Luminescent down-shifting spectral converter layers are normally deposited on the surface of the PV cell. The DS material absorbs the incident solar radiation, which is re-emitted towards the PV cell at a different, longer, wavelength. A down-shifting material absorbs UV and visible radiation typically between 300 and ~500 nm and must emit at a wavelength where the EQE of the cell is near 100% (from ~500 to ~700 nm). These re-emitted photons are then efficiently absorbed by the photovoltaic cell, generating a larger number of electron–hole pairs and thereby increasing the short-circuit current (J_{sc}).[20] Whereas, a LSC device consists of a highly transparent matrix in which highly emissive chromophores are embedded. In this case the solar radiation is absorbed by the chromophore and re-emitted in the same form as by a DSL. Because of the difference in the refractive index between the LSC surface and the air, the re-emitted radiation is guided towards the edges of the LSC, where PV cells of the appropriate size convert this radiation into electricity.[22,23]

The development of lanthanide-based luminescent materials for LSCs or LDSLs requires careful consideration of the ligand structure and coordination environment around the lanthanide ion. The choice of ligands can significantly influence the efficiency of energy transfer and the stability of the complexes under prolonged exposure to UV light. Recent advances in coordination chemistry have accelerated the design of multidentate ligands that not only enhance the absorption properties of the complexes but also provide a protective environment to enhance the photostability of the luminescent centers.[24–27] Moreover, the incorporation of such complexes into polymer matrices or nanostructured films has opened new avenues for the fabrication of robust luminescent materials that can be seamlessly integrated into existing PV architectures.[28–31]

In a previous study, we reported the characterization and optical properties of a luminescent down-shifting layer (LDSL) incorporating 2–8% of an Eu(III) complex based on 3-(diphenylphosphoryl)-1-isoquinolinecarboxylic acid, dispersed in a polyvinyl butyral (PVB) matrix.[32] In the present work, we focus our attention on its isomeric counterpart, Eu(III)1-(diphenylphosphoryl)-3-isoquinolinecarboxylic acid assessing its potential as a chromophore for LDSL applications by investigating the effect of incorporating higher concentrations of the chromophore (15%, and 30%) within PVB layers on the performance of passivated emitter rear totally diffused (PERT) solar cells.[33] Polyvinyl butyral (PVB) was selected as the host material for the preparation of the down-shifting layer due to its excellent transparency and photostability.[34] The photovoltaic performance was evaluated by measuring current–voltage (*I–V*) characteristics, incident photon-to-electron conversion efficiency (IPCE) spectra, and electrochemical impedance spectroscopy (EIS) to gain a deeper understanding of the charge transport.

2. Experimental

2.1 Synthesis

Eu(^{1}DPIQC)$_3$ was synthetized from 1-(diphenylphosphoryl) isoquinoline-3-carboxylic acid (H^{1}DPIQC) following the procedure described by Cai *et al.*[33] by deprotonation of the ligand with NaOH and one-third equivalent of $Eu(NO_3)_3\cdot 5H_2O$ in MeOH (Scheme 1). A solution of $Eu(NO_3)_3\cdot 5H_2O$ (50.0 mg, 0.117 mmol, 1.0 equiv.) in MeOH (1.5 mL) was added to a solution of H^{1}DPIQC (0.131 g, 0.350 mmol, 3.0 equiv.) and NaOH (14.1 mg, 0.350 mmol, 3.0 equiv.) in MeOH (1.5 mL) at rt, and a white solid product precipitated immediately. The mixture was filtered and washed with MeOH to afford the Eu(^{1}DPIQC)$_3$ as a white solid (0.132 g, 89%). m.p.: >300 °C. IR (cm^{-1}) ν: 3042 (C_{sp^3}–H), 1617 (C=O), 1439, 1365, 1140 (P=O), 498 (Eu–O), 383 (Eu–N) (Fig. S1 in ESI†). HRMS-ESI calculated for $C_{66}H_{45}N_3O_9EuP_3Na$ $[M + Na]^+$: 1290.1459, found 1290.1435 (Fig. S2 in ESI†).

2.2 Preparation of luminescent down-shifting layers

Two different concentrations of the Eu complex (15% and 30% w/w) were then added to a PVB solution in CH_2Cl_2 (1.0 g/6 mL) and stirred vigorously at room temperature for 30 minutes. The luminescent down-shifting layer (LDSL) films were prepared using the spin-coating method on an SPS Polos Spin 150i spin coater. Specifically, 2.5 mL of the Eu(^{1}DPIQC)$_3$/PVB/CH_2Cl_2 mixture was deposited on K9 optical glass (900 mm^2 area, 3 mm thickness). The spin-up phase was performed at 200 rpm with

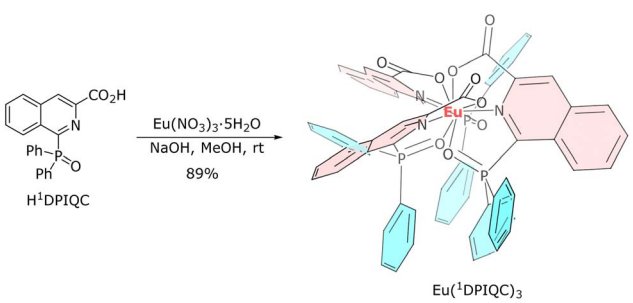

Scheme 1 Synthesis of the Eu(^{1}DPIQC)$_3$ complex.

© 2025 The Author(s). Published by the Royal Society of Chemistry

an acceleration of 100 rpm per s for 5 seconds, followed by a spin-off at 3000 rpm with an acceleration of 10 000 rpm s^{-1} for 20 seconds. Edge bead removal was done at 600 rpm with an acceleration of 1000 rpm per s over a 10 seconds interval. Finally, drying was carried out at 4000 rpm with an acceleration of 1000 rpm per s for 20 seconds.

2.3 Characterization

The excitation and emission spectra of the LDSL were recorded using a JASCO FP-850 spectrofluorometer, with all measurements performed at room temperature. To ensure consistency across experiments, the samples were weighted to maintain comparability of the spectra. The photovoltaic performance of PERT solar cells, with and without the LDSL, was evaluated at room temperature by measuring current–voltage (*I–V*) curves and incident photon-to-electron conversion efficiency (IPCE) spectra. A CT80AAA solar simulator from Photo Emission Tech, equipped with a 300 W Xe lamp, provided a standard AM 1.5 solar spectrum (one sun = 100 mW cm^{-2}). Current–voltage measurements were performed using a Keithley 2400 Source Meter, and the system was calibrated with a PET reference c-Si solar cell (model #60909). The IPCE spectra were recorded using a PET Quantum Efficiency System, equipped with two light sources for monochromatic illumination: a 300 W xenon lamp and a halogen lamp.

Electrochemical impedance spectroscopy (EIS) measurements of the bare and LDSL-coated solar cells were carried out at their open-circuit potential over a frequency range of 1×10^{-1}Hz to 5×10^{3} Hz at room temperature with an amplitude of 10 mv using an Origaflex bipotentiostat. All measurements were performed under illumination to simulate operating conditions.

The Ultraviolet (UVA and UVB) radiation was measured at the Plataforma Solar del Desierto de Atacama (PSDA), a strategic facility for the development of photovoltaic projects in northern Chile (PSDA). The PSDA, owned by the University of Antofagasta (UA) and operated by the ATAMOSTEC consortium, is located at an altitude of 1000 m.a.s.l in the Atacama Desert (24.09° S, 69.93° W). This region is characterized by a cloud cover below 3% and daily global irradiance values exceeding 8 kW h m^{-2}. It has a BWk climate according to the Köppen classification, typical of an arid cold desert zone.[35] These conditions make the PSDA an ideal natural laboratory for evaluating various pilot-scale photovoltaic (PV) technologies. To quantify UVA and UVB radiation, BASIS SUV A and B sensors from KIPP&ZONEN were used. Measurements were taken with a temporal resolution of 1 second, and the data were averaged over 1 minute intervals, covering the period from July 2023 to July 2024.

3. Results and discussion

3.1 UV-A and UV-B radiation measurement at Planta Solar Desierto Atacama (PSDA) in the Atacama Desert

In this study, the UV-A (315–400 nm) and UV-B (280–315 nm) spectral sub-bands, corresponding to the wavelengths whose photons reach the Earth's surface, were analyzed. These radiation bands are influenced by factors such as solar elevation, geographic characteristics, cloud cover, atmospheric aerosols, and ozone content.[2] The results of the analysis conducted at PSDA are presented in Fig. 1, which shows the frequency distribution of UV-A and UV-B for each season throughout the study year.

Fig. 1a and b present the frequency distribution of UV-A and UB-B irradiance, respectively, showing a clear seasonal variation. A distinct difference is noted between the colder seasons (winter and autumn) and the warmer seasons (spring and summer). In winter, the distribution is skewed toward lower values, with most irradiance events ranging between 5 and 25 W m^{-2}, indicating a reduced UV-A exposure. In contrast, spring and summer display a significant increase in the frequency of higher irradiance events, particularly above 45 W m^{-2}. During summer, the frequency reaches its peak in the 60–75 W m^{-2} range. These values are comparable to those recorded by Mondaca *et al.*, who measured UV-A irradiances exceeding 65 W m^{-2} in the Atacama Desert.[36]

Regarding the UV-B irradiance, during autumn and winter there is a predominance of low-intensity events, with frequencies exceeding 25% for values close to 0.2 W m^{-2}. In both

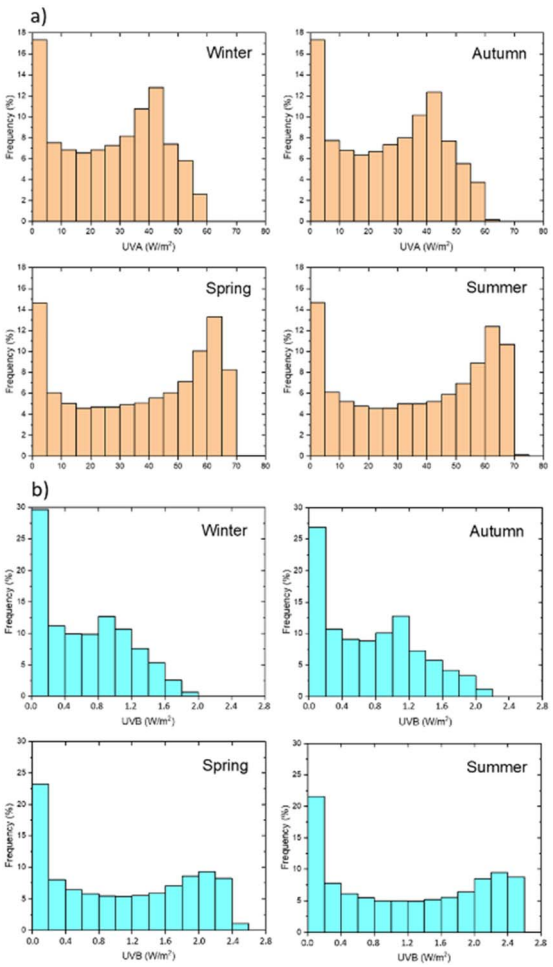

Fig. 1 Seasonal frequency distribution of UV irradiance from July 2023 to July 2024. (a) UV-A irradiance, and (b) UV-B irradiance.

© 2025 The Author(s). Published by the Royal Society of Chemistry

seasons, the distribution shows a clear decrease, indicating that most events are concentrated at low UV-B irradiances. However, events exceeding 1.2 W m^{-2} are also recorded, with some even surpassing 2.0 W m^{-2}. In contrast, during spring and summer, the distributions are more uniform, with a significant proportion of events in the intermediate and high irradiance ranges (above 2.0 W m^{-2}). In summer, a notable increase in events with values above 2.4 W m^{-2} is observed.

The measured UV-A and UV-B irradiance levels are consistent with the findings of Urrejola *et al.*, who reported that UV radiation levels in this region are 65% higher than those deemed normal or safe according to European Union regulations.[37] Such elevated radiation levels can degrade the efficiency of the encapsulants and adhesives in photovoltaic modules, leading to losses in optical transmission and electrical performance over time. This indicates that current standards for PV devices may underestimate the extreme UV radiation in the Atacama Desert. For example, the IEC 61215-2016 standard only requires UV preconditioning tests with a cumulative dose of 15 kW h m^2 (applying 50 W m^{-2} between 280 nm and 400 nm under AM 1.5 conditions), while a module in the Atacama Desert may be exposed to up to 3000 kW h m^2 over a 25 year period.[37,38] These data could be valuable in other high-irradiance regions classified under the Köppen-Geiger-photovoltaic climate methodology, such as Gibson (Australia), Almería (Spain), or Marrakesh (Morocco).[39]

3.2 Optical characterization

Eu(^{1}DPIQC)$_3$/PVB films with different concentrations of the active complex were prepared as detailed in the Experimental section below. In the following we report on the optical properties of the prepared films and the testing of their use as LSDLs. The excitation and emission spectra of the Eu(^{1}DPIQC)$_3$ complex in dichloromethane solution and in the solid state were previously reported by Cai *et al.*[33]

The luminescent excitation and emission spectra of Eu(^{1}DPIQC)$_3$/PVB films with different concentrations of the active Eu complex were examined. Fig. 2 illustrates the room temperature excitation and emission spectra for samples doped with 15% and 30% chromophore, respectively. The excitation spectra display a broad band from 240 to 350 nm, attributed to the π–π* electron transition of the ligand. The emission spectra of the complex embedded in PVB, excited at 250 nm, were analyzed for both concentrations of the Eu complex. All spectra exhibit characteristic sharp peaks associated with the $^5D_0 \rightarrow {}^7F_j$ transitions of the Eu^{3+} ion. The expected peaks for the $^5D_0 \rightarrow {}^7F_1$, $^5D_0 \rightarrow {}^7F_2$, and $^5D_0 \rightarrow {}^7F_4$ transitions are well-resolved, with the hypersensitive $^5D_0 \rightarrow {}^7F_2$ transition remarkably intense. This intensity indicates a highly polarized chemical environment surrounding the Eu^{3+} cation, responsible for the brilliant red emission (see inset, Fig. 2). The ^{1}DPIQC ligand exhibits triplet sensitivity, facilitating efficient energy transfer from the lowest excited singlet state S1, which we calculated to lie at ~33 600 cm^{-1} above the ground state, S0, to the lowest triplet state, T1, calculated to lie at ~20 000 cm^{-1} (2.48 eV).[40] These values align well with experimental data.[33] Following Latva's empirical rule, the ligand's lowest triplet energy level T_1 needs to be ~2.500 cm^{-1} above the $^5D_0$ excited state of Eu^{3+} (17 227 cm^{-1}) in order to ensure an energy transfer from the ligand to the europium cation, a condition that is satisfactorily fulfilled in the present case.[41]

As it is well known, the magnetic dipole (MD) transition $^5D_0 \rightarrow {}^7F_1$ is largely independent of the ligand field, making it a suitable internal standard for accounting for ligand variations.[42]

3.3 PV characteristics of the luminescent down-shifting layers

The photovoltaic parameters of the LDSLs were obtained using a solar simulator (AM 1.5G) as the light source. The resulting *I–V* curves are presented in Fig. 3, while the photovoltaic parameters for both the bare cell and those coated with LDSLs with varying concentrations of the Eu complex are detailed in Table 1.

The fill factors (FF) for the bare cell and the cells coated with 15% and 30% Eu complex embedded in PVB (Table 1) are found to be comparable. However, there is a notable enhancement in both the open circuit voltage (V_{oc}) and short circuit current (J_{sc}) for the cells equipped with LDSLs. This enhancement results in

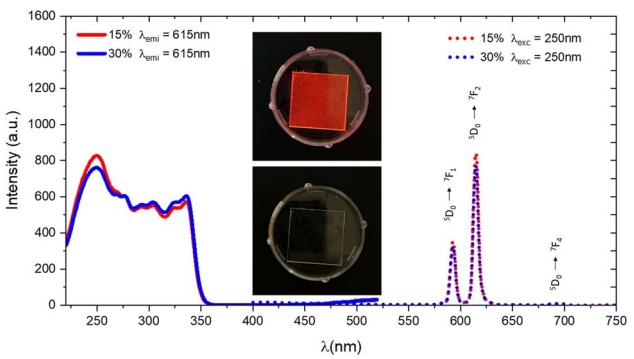

Fig. 2 Excitation (λ_{em} = 615 nm) (left) and emission spectra (λ_{ex} = 278 nm) (right) for the $^5D_0 \rightarrow {}^7F_j$ (J = 1,2,4) transitions in Eu complex in PVB films with different concentrations of Eu(^{1}DPIQC)$_3$/PVB. (Inset) Photographs of a Eu(^{1}DPIQC)$_3$/PVB film under natural day light (down) and UV illumination (up).

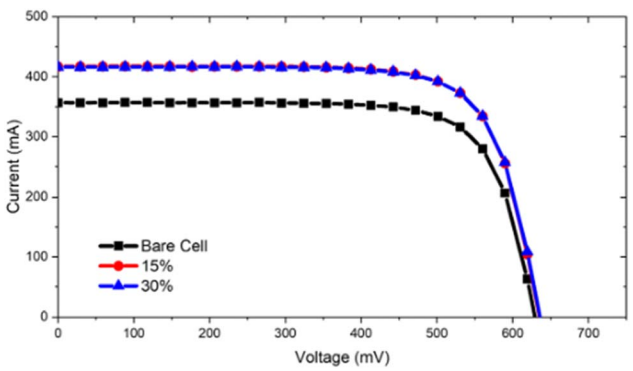

Fig. 3 *I–V* curves obtained under the irradiation of standard AM1.5G for cells with LDSLs containing different concentrations of Eu(^{1}DPIQC)$_3$ in PVB.

© 2025 The Author(s). Published by the Royal Society of Chemistry

Table 1 Variation of the photovoltaic parameter for a c-Si cell coated with Eu(^{1}DPIQC)$_3$/PVB as a function of the Eu-complex concentration. All measurements were carried out at room temperature

Eu(^{1}DPIQC)$_3$[a]	I_S (mA)	V_{oc} (mV)	J_{sc} (mA cm^{-2})	FF	P_{MAX} (mW)	η (%)
0%	345.9	630.6	28.82	0.75	169.2	14.10
15%	415.8	635.1	34.65	0.75	199.2	16.60
30%	416.3	635.7	34.69	0.75	199.4	16.62

[a] Eu complex concentration.

a power conversion efficiency (η) that is approximately 16% higher for the coated cells. The increased efficiency is primarily attributed to the down-shifting mechanism, which facilitates energy conversion by effectively harnessing higher-energy UV photons.

A comprehensive understanding of the role of luminescent down-shifting layers in enhancing the performance of photovoltaic devices can be achieved through an analysis of the IPCE curves for the cells with and without these layers, as shown in Fig. 4. The cells coated with Eu(^{1}DPIQC)$_3$/PVB films exhibit a marked improvement in photovoltaic performance in the ultraviolet (UV) spectral region.

As depicted, there is an increase in the IPCE within the UV range, specifically between 300 and 360 nm, corresponding to wavelengths where c-Si cells generally display a diminished efficiency.

The observed enhancement can be attributed to the effective conversion of high-energy UV photons into lower-energy visible photons by the LDSL through a down-shifting mechanism, increasing the number of photons available for absorption by the c-Si cell and thereby improving their overall device efficiency.

The enhanced electrical power generation from the photovoltaic device with the LDSL coating can be deduced from the following equation.[28]

$$\Delta PV = \frac{\int_0^{V_{oc}} P_{coated}\,dV - \int_0^{V_{oc}} P_{bared}\,dV}{\int_0^{V_{oc}} P_{coated}\,dV} \times 100 \quad (1)$$

where V_{oc} represents the open-circuit voltage of the photovoltaic device, P_{coated} is the power generated by the LDSL-coated device, and P_{bare} is the power generated by the uncoated c-Si cell. The results indicate an enhancement in the cell efficiency of approximately 16% for the cells coated with films containing either 15% or 30% Eu complex. Our findings suggest that Eu(III) 1-(diphenylphosphoryl)-3-isoquinolinecarboxylate exhibits photoluminescent behavior comparable to other compounds embedded in various polymers. Table 2 presents the reported EQE enhancement in the UV region for selected Eu^{3+}-based LDS coatings.

Table 2 EQE values for some Eu^{3+}-based luminescent downshifting coatings[a]

LSC layer	EQE increase (%)	Ref.
Eu(tta)$_3$(phen)/EVA	17	43
[EuL]$_3$/EVA	15	43
[Eu(tfc)$_3$:EABP] 1:1 EVA	5	44
[Eu(tfc)$_3$/Eu(dbm)$_3$phen]/PVA	5	45
Eu(^{3}DPIQC)$_3$/PVB (6% w/w)	8	32
Eu(^{1}DPIQC)$_3$/PVB (15% w/w)	17	This work

[a] EVA = ethylene-vinyl acetate; PVB = Polyvinyl butyral; L_3 = triazole-pyridine-bistetrazolate; Eu(tfc)$_3$ = tris[3-(trifluoromethylhydroxymethilene)-D-camphorate]Eu^{3+}; EABP = 4,4′-bis(diethyla-mino)benzophenone; Dbm = dibenzoylmethane; ^{1}DPICQ = 1-(diphenylphosphoryl)-3-isoquinolinecarboxylate; ^{3}DPICQ = 3-(diphenylphosphoryl)-1-isoquinolinecarboxylate.

3.4 Electrochemical characterization

Electrochemical impedance spectroscopy (EIS) was employed to characterize the behavior of the solar cells both before and after

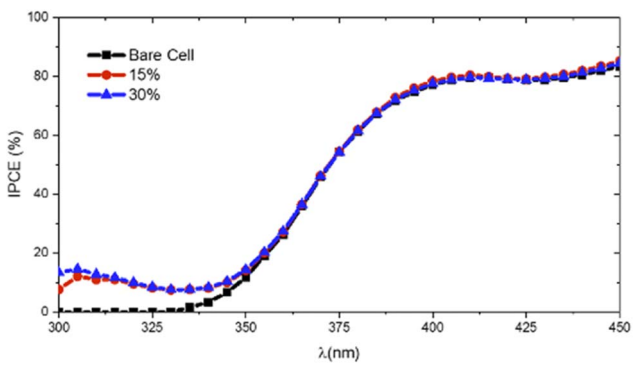

Fig. 4 IPCE curves of a c-Si with LDSLs containing different concentrations of Eu(^{1}DPIQC)$_3$/PVB.

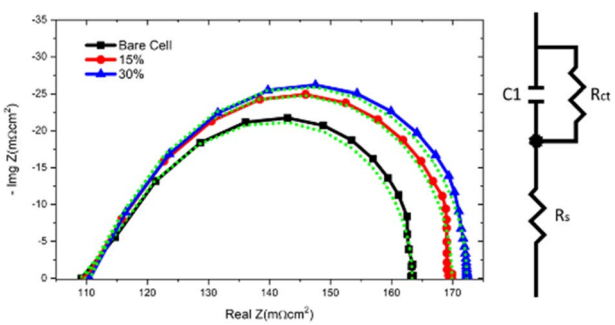

Fig. 5 Nyquist plot under illumination conditions (under irradiation of standard AM1.5G) of Eu(^{1}DPIQC)$_3$/PVB and bare c-Si cell. Green dotted curves represent the fit of the experimental curves.

© 2025 The Author(s). Published by the Royal Society of Chemistry

Table 3 EIS analysis of the PV devices with different contents of Eu(^{1}DPIQC)$_3$/PVB

Cell	R_s (mΩ cm^2)	C_1 (F cm^{-2} × 10^{-5})	R_{ct} (mΩ cm^2)	τ (μs)
Bare cell	96.676	198.31	66.693	132.52
PVB:Eu complex 15%	97.596	194.37	72.318	140.29
PVB:Eu complex 30%	97.800	189.06	74.532	140.86

the incorporation of a LDSL. The results are presented in the form of Nyquist diagrams in Fig. 5, which highlight the impedance characteristics of untreated solar cells compared to those treated with LDSLs. This analysis enables a comprehensive understanding of the charge transfer resistance, dielectric properties, and overall efficiency improvements attributable to the LDSL treatment.

The semicircles observed in these diagrams were interpreted by fitting them to an equivalent circuit model composed of resistive and capacitive (RC) elements. This fitting was performed using the specialized ZView 3.2b software, which allowed for a detailed analysis of the electrical parameters involved. The spectra obtained showed a behavior consistent with previous work, as well as with studies in which a single semicircle is characteristic of solar cells of this type.[46,47]

One of the key findings in the EIS analysis are the three fundamental parameters which can be obtained from eqn (2) and (3): the resistance of the external circuit (R_s), the recombination resistance (R_{ct}), and the junction capacitance (C_1).[48] The resistance associated with the external circuit contributions (R_s) shows a nearly constant behavior across all the samples studied (see Table 3), remaining around 97 mΩ cm^2, suggesting that the presence of the europium complex did not have a significant impact on this external resistance.

However, a very different behavior was observed in the recombination resistance (R_{ct}), which is related to the charge recombination processes within the device. In the cells without LDSL, the R_{ct} value was 66.693 mΩ cm^2. In contrast, when incorporating 15% of the Eu complex, R_{ct} increased to 72.318 mΩ cm^2. For 30% of the Eu complex, the values rose to 74.532 mΩ cm^2, suggesting that the incorporation of this complex improves the charge transport efficiency, likely by reducing recombination losses at the interface between the active layers.

$$Z'(\omega) = R_s + \frac{R_{ct}}{1 + (C_1 \omega R_{ct})^2} \quad (2)$$

$$Z''(\omega) = -\frac{R_{ct}{}^2 \omega C_1}{1 + (C_1 \omega R_{ct})^2} \quad (3)$$

On the other hand, no significant increase in the recombination resistance was observed when concentrations were raised above 30%, indicating that the Eu complex, at a concentration of 30%, could minimize some structural effects present in the cell, generating an inductive effect by passivating its interface, contributing to the improvement of electrochemical parameters such as the overall efficiency of the cell. These results suggest a slightly better photovoltaic performance for films with a 30%, of Eu complex.

In addition to the impact on the resistances, the junction capacitance (C_1) and the spatial charge distribution in the depletion region of the device showed insignificant variations after the incorporation of the LDSL. Only a slight decrease was detected when the LDSL was added at either 15% or 30% Eu concentrations, which reinforces the idea that the presence of the Eu complex at a concentration of 30% does not affect the cell's light absorption, but improves the electron retention in the semiconductor's conduction band, reducing recombination and allowing an increase in the short-circuit current, thus improving the overall performance of the device.

This statement can be corroborated through the analysis of the electron recombination time constant (τ) to determine the minority carrier lifetime, where values of 132.52, 140.29, and 140.94 μs (see Table 3) were found for the untreated cell, and the cells with 15% and 30% europium complex, respectively. These results indicate that, at a concentration of 30%, the europium complex can minimize the recombination and help the electrons to remain in the semiconductor conduction band for a longer time. These conclusions are consistent with former bibliographic reports[48–50] and the parameters measured in this study, such as short-circuit current (J_{sc}), open-circuit voltage (V_{oc}), and incident photon-to-electron conversion efficiency (IPCE), which also showed improvements in the cells with 30% Eu compared to the bare cell.

These experiments confirm thus that the inclusion of the Eu complex at a concentration of 30% is beneficial for improving the conversion efficiency of c-Si solar cells, while higher concentrations could lead to negative effects due to the formation of defects at the interface.

4. Conclusions

In this work, we report on the performance of luminescent down-shifting layer (LDSL) coatings based on Eu^{3+} organic–inorganic hybrid materials (Eu(^{1}DPIQC)$_3$/PVB) for c-Si solar cells. We have shown that these materials can efficiently absorb the extreme UVA and UVB solar irradiance found in the Atacama Desert. When coupled to a crystalline silicon (c-Si) solar cell, the LDSL effectively absorbs the UV portion of the solar spectrum, converting it into visible light that can be absorbed by the cell. This conversion significantly enhances the cell's performance, as demonstrated by an efficiency increase from 14.10% (bare cell) to 16.62% with a 30% concentration of the Eu-complex embedded in PVB.

Additionally, the IPCE spectra of the photovoltaic devices showed an improved spectral response between 200–350 nm. An electrochemical impedance spectroscopy (EIS) analysis revealed that the series resistance (R_s) remained stable across all

© 2025 The Author(s). Published by the Royal Society of Chemistry

samples (~97 mΩ cm^2), while the recombination resistance (R_{ct}) increased with the incorporation of 15% or 30% Eu-complex, indicating a better charge transport in these cases. A better performance was observed for a LSDL with 30% Eu-complex, where recombination losses were reduced, leading to higher efficiency. Moreover, the electron recombination time increased, further boosting photovoltaic performance under AM 1.5G conditions, confirming the overall positive effect of the Eu-complex on the performance of the solar cell. All together these results suggest that incorporating LDSL coatings can help in reducing electron–hole pair thermalization losses within the solar cell, as these losses are instead absorbed by the LDSL.

Data availability

The data underlying this study are available in this article and its ESI.†

Author contributions

D. Espinoza: investigation; R. Nelson: conceptualization, investigation, writing; F. Vargas: investigation; A. Mestra: conceptualization, writing-review; L. Sánchez-Muñoz: investigation, validation; P. Alemany: validation, conceptualization, writing – review and editing; D. Olivares, investigation, validation; L. Conde: investigation; J. Llanos: conceptualization, methodology, investigation, project administration; writing-review.

Conflicts of interest

There are no conflicts to declare.

Acknowledgements

The authors acknowledge the financial support of the Agencia Nacional Investigación y Desarrollo (ANID) Chile, grant 1220159, and ANID/FONDAP 1523A0006, MICIU (Spain), grant PID2021-128217NB-I00, and Generalitat de Catalunya, grant 2021SGR00286. P. A. and L. S.-M. also received support from the Maria de Maeztu Units of Excellence Program, grant CEX2021-001202-M. J. L. would also like to thank "Núcleo de materiales funcionales" No. 8 UCN-VRIDT 076/2020, for scientific support.

Notes and references

1 R. R. Cordero, A. Damiani, G. Seckmeyer, J. Jorquera, M. Caballero, P. Rowe, J. Ferrer, R. Mubarak, J. Carrasco, R. Rondanelli, M. Matus and D. Laroze, *Sci. Rep.*, 2016, **6**, 22457.

2 R. R. Cordero, A. Damiani, J. Jorquera, E. Sepúlveda, M. Caballero, S. Fernandez, S. Feron, P. J. Llanillo, J. Carrasco, D. Laroze and F. Labbe, *Antonie van Leeuwenhoek*, 2018, **111**, 1301–1313.

3 J. Nikoletatos and G. Halambalakis, in *McEvoy's Handbook of Photovoltaics: Fundamentals and Applications*, ed. S. A. Kalogirou, Elsevier Ltd, 2018, pp. 1155–1182.

4 C. R. Osterwald, in *Practical Handbook of Photovoltaics*, ed. L. C. Augustin McEvoy and T. Markvart, Elsevier Ltd, 2012, pp. 1045–1069.

5 A. Sinha, J. Qian, S. L. Moffitt, K. Hurst, K. Terwilliger, D. C. Miller, L. T. Schelhas and P. Hacke, *Prog. Photovolt.: Res. Appl.*, 2023, **31**, 36–51.

6 J. Kettle, M. Aghaei, S. Ahmad, A. Fairbrother, S. Irvine, J. J. Jacobsson, S. Kazim, V. Kazukauskas, D. Lamb, K. Lobato, G. A. Mousdis, G. Oreski, A. Reinders, J. Schmitz, P. Yilmaz and M. J. Theelen, *Prog. Photovolt.: Res. Appl.*, 2022, **30**, 1365–1392.

7 P. Yang, S. Razzaq, R. Jiao, Y. Hu, L. Liu and J. Tao, *J. Sol. Energy Res. Updates*, 2023, **10**, 36–45.

8 D. S. Ruby and W. K. Schubert, *Conf. Rec. IEEE Photovolt. Spec. Conf.*, 1991, **1**, 111–117.

9 S. H. Park, S. Ahn, J. Gwak, K. Shin, S. K. Ahn, K. Yoon, Y. Cho, D. W. Kim and J. H. Yun, *Curr. Appl. Phys.*, 2013, **13**, 1684–1688.

10 R. Ilmi, N. Hasan, J. Liu, D. Mara, R. Van Deun and K. Iftikhar, *J. Photochem. Photobiol., A*, 2017, **347**, 116–129.

11 R. Ilmi, S. Kansız, N. K. Al Rasbi, J. Husband, N. Dege and M. S. Khan, *Polyhedron*, 2023, **246**, 116673.

12 R. Ilmi and K. Iftikhar, *J. Photochem. Photobiol., A*, 2016, **325**, 68–82.

13 R. Ilmi, A. B. Ganaie and K. Iftikhar, *J. Mol. Struct.*, 2018, **1173**, 990–999.

14 G. Maggioni, A. Campagnaro, M. Tonezzer, S. Carturan and A. Quaranta, *ChemPhysChem*, 2013, **14**, 1853–1863.

15 N. T. Kalyani, S. J. Dhoble and R. B. Pode, *Luminescence*, 2013, **28**, 183–189.

16 B. González-Díaz, M. H. Saw, C. Hernández-Rodríguez, J. Sanchiz, Y. S. Khoo and R. Guerrero-Lemus, *Mater. Sci. Eng., B*, 2020, **261**, 114763.

17 D. A. R. Barkhouse, O. Gunawan, T. Gokmen, T. K. Todorov and D. B. Mitzi, *Prog. Photovolt.: Res. Appl.*, 2015, **24**, 1251–1260.

18 A. R. Frias, M. A. Cardoso, A. R. N. Bastos, S. F. H. Correia, P. S. André, L. D. Carlos, V. de Z. Bermudez and R. A. S. Ferreira, *Energies*, 2019, **12**, 451.

19 C. L. Mulder, L. Theogarajan, M. Currie, J. K. Mapel, M. A. Baldo, M. Vaughn, P. Willard, B. D. Bruce, M. W. Moss, C. E. McLain and J. P. Morseman, *Adv. Mater.*, 2009, **21**, 3181–3185.

20 E. Klampaftis, D. Ross, K. R. McIntosh and B. S. Richards, *Sol. Energy Mater. Sol. Cells*, 2009, **93**, 1182–1194.

21 M. A. Cardoso, S. F. H. Correia, A. R. Frias, H. M. R. Gonçalves, R. F. P. Pereira, S. C. Nunes, M. Armand, P. S. André, V. de Zea Bermudez and R. A. S. Ferreira, *J. Rare Earths*, 2020, **38**, 531–538.

22 M. K. Assadi, H. Hanaei, N. M. Mohamed, R. Saidur, S. Bakhoda, R. Bashiri and M. Moayedfar, *Appl. Phys. A:Mater. Sci. Process.*, 2016, **122**, 1–12.

23 M. Rafiee, S. Chandra, H. Ahmed and S. J. McCormack, *Opt. Mater.*, 2019, **91**, 212–227.

24 D. Yang, H. Liang, Y. Liu, M. Hou, L. Kan, Y. Yang and Z. Zang, *Dalton Trans.*, 2020, **49**, 4725–4731.

© 2025 The Author(s). Published by the Royal Society of Chemistry

25 D. Yang, Y. Wang, Z. Li, Y. Xu, F. Cheng, P. Li and H. Li, *J. Mater. Chem. C*, 2018, **6**, 1153–1159.
26 D. Yang, Y. Wang, Y. Wang, Z. Li and H. Li, *ACS Appl. Mater. Interfaces*, 2015, **7**, 2097–2103.
27 D. Yang, Y. Wang, L. He and H. Li, *ACS Appl. Mater. Interfaces*, 2016, **8**, 19709–19715.
28 S. F. H. Correia, A. R. N. Bastos, L. S. Fu, L. D. Carlos, P. S. André and R. A. S. Ferreira, *Opto-Electron. Adv.*, 2019, **2**, 190006.
29 O. Moudam, B. C. Rowan, M. Alamiry, P. Richardson, B. S. Richards, A. C. Jones and N. Robertson, *Chem. Commun.*, 2009, 6649–6651.
30 Q. Ru, J. Chen and H. Li, *Opt. Mater.*, 2024, **155**, 115794.
31 D. Yang, H. Li and H. Li, *Coord. Chem. Rev.*, 2024, **514**, 215875.
32 F. Vargas, R. Nelson, D. Espinoza, I. Brito, L. Sánchez-Muñoz, P. Alemany, S. Ortiz, P. Ferrada, A. Mestra and J. Llanos, *Molecules*, 2023, **28**, 7924.
33 Z. Cai, C. Wei, B. Sun, H. Wei, Z. Liu, Z. Bian and C. Huang, *Inorg. Chem. Front.*, 2021, **8**, 41–47.
34 X. Wang, T. Wang, X. Tian, L. Wang, W. Wu, Y. Luo and Q. Zhang, *Sol. Energy*, 2011, **85**, 2179–2184.
35 D. Olivares, P. Ferrada, A. Marzo, J. Llanos, C. Miranda-Ostojic, V. del Campo, S. Bravo and E. Fuentealba, *Sol. Energy Mater. Sol. Cells*, 2021, **227**, 111109.
36 G. Mondaca, M. Trigo-González, A. Marzo, J. Alonso-Montesinos, J. Barbero, G. Salazar, D. Olivares and P. Ferrada, *Proceedings of the ISES Solar World Congress 2019 and IEA SHC International Conference on Solar Heating and Cooling for Buildings and Industry 2019*, 2020, pp. 365–375.
37 E. Urrejola, J. Tapia, M. J. Riquelme, D. Muñoz, R. Kopecek and E. Fuentealba-Vidal, *37th European Photovoltaic Solar Energy Conference and Exhibition*, 2020, pp. 1033–1037.
38 J. F. Lelièvre, R. Couderc, N. Pinochet, L. Sicot, D. Munoz, R. Kopecek, P. Ferrada, A. Marzo, D. Olivares, F. Valencia and E. Urrejola, *Sol. Energy Mater. Sol. Cells*, 2022, **236**, 111508.
39 J. Ascencio-Vásquez, K. Brecl and M. Topič, *Sol. Energy*, 2019, **191**, 672–685.
40 L. Sánchez-Muñoz, D. Aravena, J. Cirera and P. Alemany, *ChemPhysChem*, 2025. submitted for publication.
41 M. Latva, H. Takalob, V. M. Mukkala, C. Matachescu, J. C. Rodríguez-Ubis and J. Kankare, *J. Lumin.*, 1997, **75**, 149–169.
42 X. Zhang, S. Wen, S. Hu, L. Zhang and L. Liu, *J. Rare Earths*, 2010, **28**, 333–339.
43 T. Fix, A. Nonat, D. Imbert, S. Di Pietro, M. Mazzanti, L. J. Charbonnière and A. Slaoui, *Prog. Photovolt.: Res. Appl.*, 2016, **24**, 1251–1260.
44 A. Le Donne, M. Dilda, M. Crippa, M. Acciarri and S. Binetti, *Opt. Mater.*, 2011, **33**, 1012–1014.
45 A. Le Donne, M. Acciarri, D. Narducci, S. Marchionna and S. Binetti, *Prog. Photovolt.: Res. Appl.*, 2009, **17**, 519–525.
46 K. K. Markose, M. Jasna, P. P. Subha, A. Antony and M. K. Jayaraj, *Sol. Energy*, 2020, **211**, 158–166.
47 A. Srivastava, D. Sharma and S. K. Srivastava, *Org. Electron.*, 2023, **119**, 106817.
48 A. C. Lazanas and M. I. Prodromidis, *ACS Meas. Sci. Au*, 2023, **3**, 162–193.
49 Q. Wang, J.-E. Moser and M. Grätzel, *J. Phys. Chem. B*, 2005, **109**, 14945–14953.
50 B. Roose, K. Dey, M. R. Fitzsimmons, Y. H. Chiang, P. J. Cameron and S. D. Stranks, *ACS Energy Lett.*, 2024, **9**, 442–453.

© 2025 The Author(s). Published by the Royal Society of Chemistry